NANO LETTERS

2007
Vol. 7, No. 8
2346−2350

Nanoparticle-Mediated Coupling of Light into a Nanowire

Mark W. Knight,[†] Nathaniel K. Grady,[†] Rizia Bardhan,[‡] Feng Hao,[§] Peter Nordlander,[||] and Naomi J. Halas*

Department of Electrical and Computer Engineering, Department of Chemistry, Department of Physics and Astronomy, and the Laboratory for Nanophotonics, Rice University, 6100 Main Street, Houston, Texas 77005

Received April 27, 2007; Revised Manuscript Received June 4, 2007

ABSTRACT

We show that a nanoparticle can serve as an efficient antenna for coupling of visible light into propagating plasmons of an Ag nanowire. For long wires, the coupling is maximal for incident light polarized perpendicular to the nanowire. For sub-10-μm nanowires, the polarization corresponding to maximum emission from the ends of the nanowire was found to be strongly dependent on the nanowire geometry and position of the vicinal nanoparticle. This nanoparticle antenna-based approach offers a potential strategy for optimizing plasmon coupling into nanoscale metallic waveguides.

The controlled coupling of light and nanoscale optical components, such as plasmonic waveguides, is a topic of intense theoretical and practical interest. Electronic integrated circuits are currently routinely manufactured with dimensions below 100 nm, where the resulting decrease in gate delays due to size reduction has led to a new regime of electronic interconnect delay-limited performance.[1] Optical interconnects could potentially support increased data transmission rates of more than a thousand times that of current electronic interconnects, provided they could be integrated on-chip and fabricated at dimensions significantly smaller than the optical diffraction limit.[2] Such integration may be possible using surface plasmon-based optics (plasmonics), where signals are transmitted by collective electronic oscillations confined to metal−dielectric interfaces. Thus far, plasmon waveguiding has been demonstrated in nanoscale metallic dot arrays,[3,4] metal−insulator−metal (MIM) structures,[5−7] and metallic nanowires.[8−11]

Efficient coupling of light into, and out of, plasmon waveguides by compensation of the momentum difference between photons and plasmons presents a critical challenge. Methods of optical signal injection into plasmonic waveguides include excitation at waveguide defects,[5,8,11,12] bends,[11] crossed wire junctions,[11,13,14] and evanescent wave excitation using the Kretschmann geometry.[10,15] It has recently been shown that plasmons on adjacent nanostructures mix and hybridize, yielding new "hybridized" plasmon states in complex systems.[16] Plasmon hybridization is also responsible for the coupling between discrete plasmons on metallic nanoparticles with the propagating plasmons supported by metallic films or wires.[16,17] It has recently been predicted that a metallic nanoparticle in close proximity to a metallic nanowire should function as an antenna at infrared and optical frequencies, providing a coupling mechanism between free-space photons and nanowire plasmons with enhanced efficiencies relative to direct optical excitation.[18] This spatially compact geometry allows for direct coupling into straight, continuous nanoscale wires and is therefore an ideal candidate for photonic input and output ports on dense, integrated plasmonic circuitry.

Here we report the experimental observation of metallic nanoparticle-mediated coupling of visible light with propagating plasmons in directly adjacent metallic nanowires. Visible light is focused onto individual nanowire−nanoparticle junctions. The plasmon resonance of the interacting nanoparticle−nanowire system provides sufficient coupling of light into the nanowire to excite propagating plasmons. Nanowire plasmons are also converted back to free-space photons at these nanoparticle−nanowire junctions, as well as at kinks and at the ends of the nanowire.[11] This assortment of plasmon launching and scattering sites allows us to examine the relative plasmon coupling efficiencies of these geometries and also provides probe sites for examining the polarization dependence of plasmon excitation on nanowires of various lengths and conformations by using optical microscopy.

The crystalline Ag nanowires that serve as waveguides in this study were synthesized using room-temperature chemical

* Corresponding author. E-mail: halas@rice.edu. Address: Department of Electrical and Computer Engineering, Department of Chemistry, Department of Bioengineering, Laboratory for Nanophotonics.

[†] Department of Electrical and Computer Engineering, Laboratory for Nanophotonics.

[‡] Department of Chemistry, Laboratory for Nanophotonics.

[§] Department of Physics and Astronomy, Laboratory for Nanophotonics.

[||] Department of Physics and Astronomy, Department of Electrical and Computer Engineering, Laboratory for Nanophotonics.

10.1021/nl071001t CCC: $37.00 © 2007 American Chemical Society
Published on Web 07/13/2007

fabrication, yielding nanowires with a mean diameter of ~220 nm and lengths ranging from 1 to 25 μm.[19] Platinum seed was formed by reducing $PtCl_2$ with ethylene glycol (EG) at 160 ± 3 °C, then adding $AgNO_3$ and poly(vinyl pyrrolidone) (PVP) dropwise over the course of 6 min. After the $AgNO_3$ was completely reduced (~60 min), the solution was cooled, washed via centrifugation once in acetone to remove EG, then twice in ethanol to remove PVP. The spherical Ag nanoparticles serving as antennas had diameters varying from 200 to 700 nm and were cofabricated in the same chemical synthesis procedure as the nanowires, remaining in solution with the nanowires following centrifugation.

Samples for these studies were prepared by drop-casting a dilute ethanolic suspension of this Ag nanowire−nanoparticle mixture on glass slides patterned with indexed grids and letting them dry under ambient conditions. A small percentage of the colloidal Ag nanoparticles were observed to deposit within ~10 nm of the nanowires. To characterize the coupling behavior, individual nanowire−nanoparticle junctions were positioned near the intensity maximum of a diffraction-limited laser spot (λ = 633 nm) using a piezoelectric stage (Nanonics Imaging Ltd., 3D Flat Scanner) mounted on an inverted optical microscope (Zeiss Axiovert 200 MAT). Polarization control of the laser light was achieved using a Glan−Thompson polarizing beamsplitter cube followed by a λ/2 plate (multi-order, 633 nm) in a rotation mount. The polarized, collimated laser beam was directed into the microscope using a half-silvered mirror and focused to a diffraction-limited spot in the image plane using a 100× objective lens (Zeiss, NA = 0.9). Light scattered from the sample passed through a half-silvered mirror and was detected using a CCD (Axiocam MRm, 1388 × 1040 pixels, spectral range 350−1000 nm). Rotating the λ/2 plate before recording each far-field image allowed the construction of curves showing relative far-field intensity as a function of laser polarization angle. High-resolution images of the individual nanowire−nanoparticle pairs were obtained using scanning electron microscopy (SEM, FEI XL-30).

In Figure 1, an individual nanowire with an adjacent Ag nanoparticle allows us to examine nanoparticle−nanowire coupling, as well as other input and output coupling mechanisms, all in a single nanostructure complex. In Figure 1A, the nanoparticle−nanowire junction is illuminated with a diffraction-limited beam spot, and emission can be observed from the nanowire terminus closest to the excitation junction. The wire plasmon wavelength in this sample was found to be 440 ± 5 nm, determined by measuring the distance between successive standing-wave peaks in the near-field intensity profile observed using collection-mode near-field scanning optical microscopy (NSOM). Previous measurements have reported decay lengths for nanowire plasmons on similar structures of 3−10 μm,[9,11,20] a length scale consistent with the observation of emission only at the nanowire terminus nearest to the plasmon launch site. When the launch geometry is reversed, that is, illumination at the end of the nanowire, emission is observed at the nanoparticle−nanowire coupling site (Figure 1B). A kink in the nanowire can also serve as a coupling site for nanowire

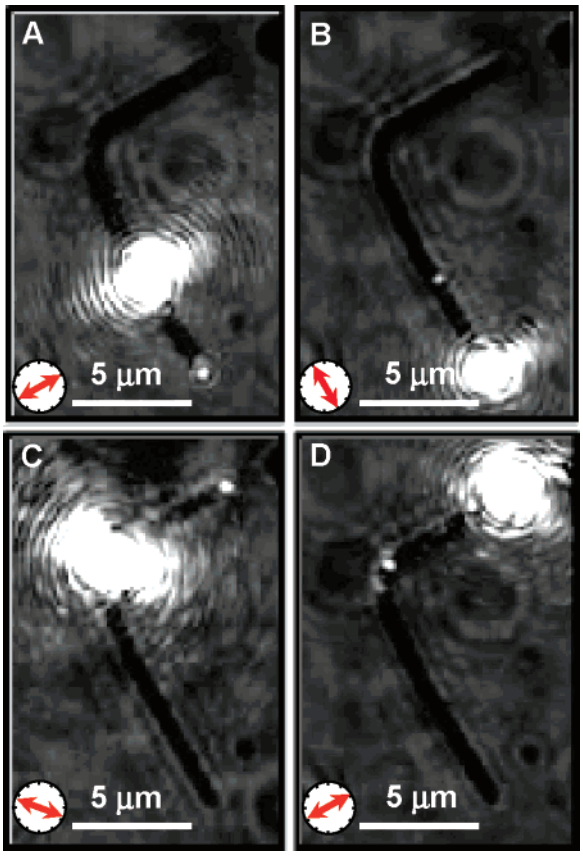

Figure 1. Optical images obtained in bright field microscopy showing coupling between free-space photons and nanowire plasmons at multiple points of broken symmetry. The large (diameter > 2 μm) laser spot was used to excite propagating wire plasmons by illumination at (A) a 216 nm diameter metallic particle adjacent to the nanowires, (B) at one end of the nanowire, (C) at the kink, and (D) at the other end of the nanowire. Red arrows indicate the laser spot polarization corresponding to maximum nanowire plasmon emission.

plasmon excitation (Figure 1C) and emission (Figure 1D). In this specific example, the kink in the nanowire consisted of two bends, separated by 900 nm, with angles of 136° and 147° (Figure 2A). The associated dipole moment can be anticipated to be weak relative to end- or particle-coupling geometries, and indeed, it was observed that higher laser excitation powers were necessary for exciting visible remote emission from the kink relative to either the nanoparticle or end-coupling geometries.

The coupling strength was measured by illuminating the wire−particle junction with a linearly polarized, diffraction-limited laser spot (Figure 2). For each polarization, the emission intensity for a given coupling site was determined by averaging the three brightest pixels at that site; small variations in reflectance coefficients for TE and TM polarizations were corrected for numerically. Data were obtained for multiple orientations of the same wire relative to the microscope to ensure that the calibrated intensity curves resulted from the coupling geometries and were not generated as artifacts of the optical setup. The 16.67 μm wire shown in Figure 2 was excited at the nanowire−nanoparticle junction (Figure 2A, site b), with observations recorded at the three remote coupling sites (a, c, and d). Data was taken

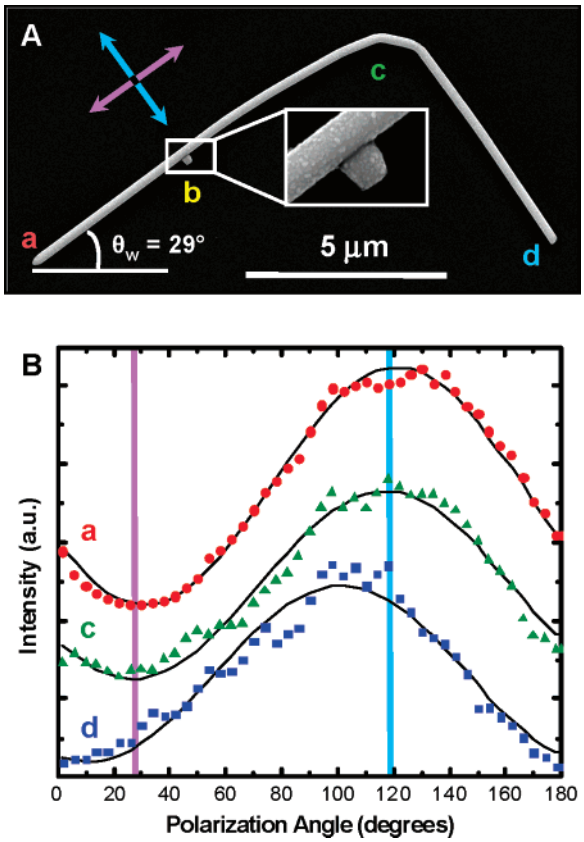

Figure 2. Polarization dependence of coupling efficiency at nanowire/particle junction. (A) SEM of silver nanoparticle (diameter = 216 nm) adjacent to a bent silver nanowire (length = 16.65 μm, width = 222 nm). Propagating plasmons were excited at the wire−particle junction (b) by a diffraction-limited laser spot (λ = 633 nm). (B) Far-field emission intensities as a function of laser polarization angle (normalized and vertically offset for clarity). Strongest coupling observed for polarization perpendicular to the wire (light blue); weakest coupling occurs when polarization is parallel to the wire (purple). Black lines are best-fit sine curves.

using low power for site a to avoid saturating the detector; a second dataset was taken with higher power levels to improve the signal/noise ratio for the weaker emission observed at sites c and d. Figure 2B shows that coupling maxima and minima correspond to laser polarizations perpendicular and parallel to the wire, respectively. The polarization dependence corresponding to the maximum plasmon emission at the remote sampling sites on the nanowire is in agreement with theory, which predicts maximum coupling for light polarized across the nanoparticle wire junction.[18] Far-field emission curves from remote sites as a function of polarization angle are well described by a simple sinusoidal dependence, $I(\theta) = I_0 \cos(2\theta + \phi_{phase}) + I_{offset}$, with a period of 180° and maxima at ϕ_{phase} (Figure 2B) (here I_{offset} is a fit parameter that scales the mean intensity averaged over all measured polarizations). It is interesting to note the shift in polarization for the distal end (site d) coupling peak, to 102 ± 4°, from the coupling maxima observed at the other emission sites.

For shorter nanowires, the polarization dependence of the far-field nanowire plasmon emission was found to be highly sensitive to junction position and nanowire length. Nanowires and nanoparticle−nanowire junctions were measured with various degrees of oxide coatings that appeared subsequent to sample preparation; however, it is important to note that this oxidation of the nanowire−nanoparticle junction structures was found to have negligible effect on the coupling efficiencies (Figure 3A,B). In Figure 3C, the end excitation of nanowire plasmons with emission from both the centrally positioned nanoparticle−nanowire junction as well as the emission from the opposite end of the nanowire are shown. In Figure 3D, the central nanoparticle−nanowire junction is illuminated, resulting in emission from both ends of the nanowire. In each of these two excitation geometries we observe the relative polarization dependence of the two plasmon "output ports" of the nanostructure. Figure 3E shows the polarization dependence of the two emission sites of the excitation geometry for the nanostructure shown in Figure 3C, while in Figure 3F the polarization dependence corresponding to structure and excitation geometry of Figure 3D are displayed.

Finite element analysis simulations using commercial software (COMSOL Multiphysics) were used to study both excitation geometries shown in Figure 3C,D (Figure 4). The nanowire and nanoparticle were modeled using a simple rod and sphere of the same dimensions as the nanowire−nanoparticle pair shown in Figure 3B. The simulation space was surrounded by scattering boundaries. A polarized Gaussian beam (beam waist = 2 μm) was simulated as the excitation source (Figure 4A,B). For a given source polarization the emission intensities at remote sites were calculated by applying far-field transforms to the wire at each point of broken symmetry. The theoretical emission curves were normalized for comparison to experimental measurements. In this study it was found that varying the wire length by less than 40 nm can significantly alter the relative polarization dependence of the observed emission. This effect may quite possibly be due to the fact that short nanowires can function as Fabry−Pérot cavities resulting in geometry specific standing plasmon waves,[9,20] where the resonant modes are selected by the laser polarization angle. The experimental and theoretical curve peaks agree to within 20° or less, where the discrepancy is likely due to uncertainties in the exact dimensions of the physical nanowire. (Surface oxide coating the nanoparticle and nanowire limited the measurement accuracy of the system dimensions.) Experimentally, this interpretation is supported by the observation that plasmons launched from wire ends always yield remote emission curves with maxima and minima corresponding to polarizations aligned longitudinally and transverse to the nanowire, respectively. This is the expected behavior for a coupling modality with a fixed plasmon launching phase (Figure 3E). Also in agreement with the Fabry−Pérot cavity interpretation, the emission peak offsets disappear for long wires because Ohmic and radiative losses decrease the amplitude of the interfering plasmons.

In summary, we have demonstrated that a metallic nanoparticle near a metallic wire can serve as an antenna enabling efficient in and out coupling of light and plasmons.

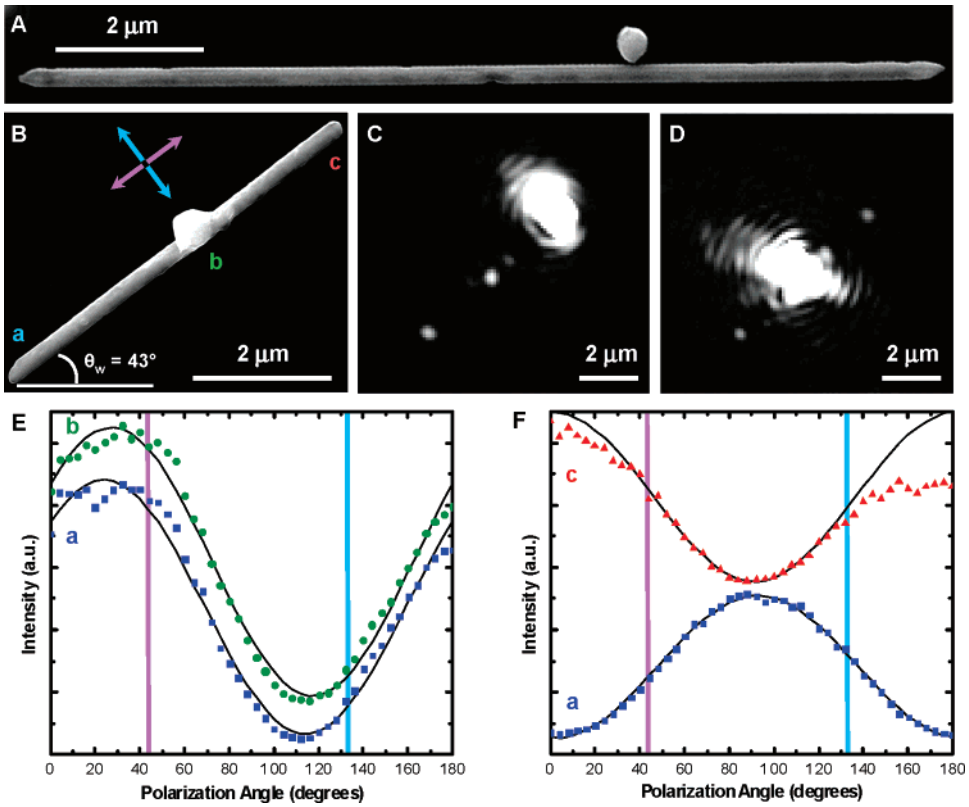

Figure 3. Geometry dependence of polarization angle for maximum far-field emission intensity (normalized and offset for clarity). (A) SEM of representative coupled silver nanowire/particle pair prior to oxidation. (B) SEM of wire used in (C−F). Wire length = 5.96 μm, diameter = 259 nm. Particle diameter = 660 nm. (C) Optical images of light coupled into nanowire through the end of nanowire and (D) through the nanowire−nanoparticle junction. (E) Emission intensities from remote coupling sites (a) and (b) when illuminated at end of nanowire (c). (F) Emission intensities from (a) and (c) when illuminated at the nanowire−nanoparticle junction (b). Black lines are best-fit sine curves.

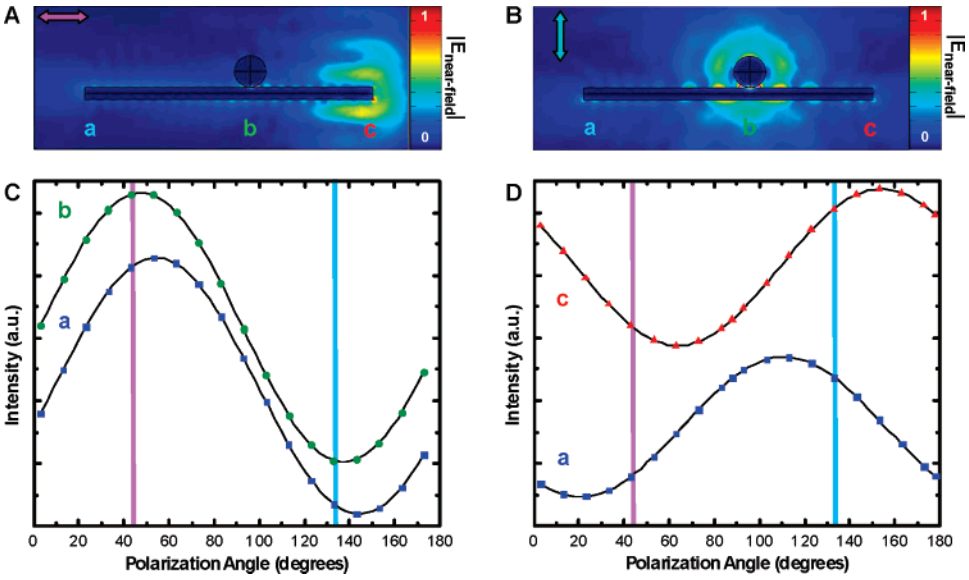

Figure 4. Finite-element analysis of nanowire−nanoparticle geometry shown in Figure 3B. (A) Near-field amplitude of the electric field for end excitation with polarization along wire (purple) and (B) particle excitation with polarization perpendicular to wire (light blue). (C) Emission intensities from remote coupling sites (a) and (b) when illuminated at the end of the wire, and (D) Emission intensities from (a) and (c) when illuminated at the nanowire−particle junction. Black lines are best-fit sine curves.

Emission amplitudes from remote coupling sites depend strongly on polarization for all wire lengths. For long wires (length > 10 μm) plasmon emission at the ends of the nanowire is strongly polarization dependent, with maximum emission corresponding to polarization transverse to the nanowire axis. Short nanowire far-field emission is highly dependent on the nanowire−nanoparticle geometry. This nanoparticle-mediated plasmon coupling geometry may prove

to be ideal for optical input and output ports on dense integrated plasmonic circuitry. This geometry may also give rise to nanoscale plasmon-based interferometers, or other standing-wave plasmon-based passive or active optical components.

Acknowledgment. This work was supported by the Air Force Office of Scientific Research (FA9550-06-1-0021), the National Science Foundation (NSF) grant EEC-0304097, the Multidisciplinary University Research Initiative (MURI) grant W911NF-04-01-0203, and the Robert A. Welch Foundation (C-1220 and C-1222). We gratefully acknowledge Avi Israel (Nanonics Imaging, Ltd.) for his assistance with near-field measurements.

References

(1) Kobrinsky, M. J.; Block, B. A.; Zheng, J.-F.; Barnett, B. C.; Mohammed, E.; Reshotko, M.; Robertson, F.; List, S.; Young, I.; Cadien, K. *Intel. Technol. J.* **2004**, *8*, 129−143.
(2) Ozbay, E. *Science* **2006**, *311*, 189−193.
(3) Maier, S. A.; Friedman, M. D.; Barclay, P. E.; Painter, O. *Appl. Phys. Lett.* **2005**, *86*, 071103.
(4) Qu, D.; Grischkowsky, D. *Phys. Rev. Lett.* **2004**, *93*, 196804.
(5) Pile, D. F. P.; Gramotnev, D. K. *Opt. Lett.* **2004**, *29*, 1069−1071.
(6) Bozhevolnyi, S. I.; Volkov, V. S.; Devaux, E.; Laluet, J. Y.; Ebbesen, T. W. *Nature* **2006**, *440*, 508−511.
(7) Lamprecht, B.; Krenn, J. R.; Schider, G.; Ditlbacher, H.; Salerno, M.; Felidj, N.; Leitner, A.; Aussenegg, F. R.; Weeber, J. C. *Appl. Phys. Lett.* **2001**, *79*, 51−53.
(8) Graff, A.; Wagner, D.; Ditlbacher, H.; Kreibig, U. *Eur. Phys. J. D* **2005**, *34*, 263−269.
(9) Ditlbacher, H.; Hohenau, A.; Wagner, D.; Kreibig, U.; Rogers, M.; Hofer, F.; Aussenegg, F. R.; Krenn, J. R. *Phys. Rev. Lett.* **2005**, *9525*, 7403−7403.
(10) Krenn, J. R.; Weeber, J. C. *Philos. Trans. R. Soc. London, Ser. A* **2004**, *362*, 739−756.
(11) Sanders, A. W.; Routenberg, D. A.; Wiley, B. J.; Xia, Y. N.; Dufresne, E. R.; Reed, M. A. *Nano Lett.* **2006**, *6*, 1822−1826.
(12) Félidj, N.; Laurent, G.; Grand, J.; Aubard, J.; Lévi, G.; Hohenau, A.; Aussenegg, F. R.; Krenn, J. R. *Plasmonics* **2006**, *1*, 35−39.
(13) Deibel, J. A.; Wang, K. L.; Escarra, M. D.; Mittleman, D. M. *Opt. Express* **2006**, *14*, 279−290.
(14) Wang, K. L.; Mittleman, D. M. *Nature* **2004**, *432*, 376−379.
(15) Kretschmann, E. *Z. Phys.* **1971**, *241*, 313−324.
(16) Wang, H.; Brandl, D.; Nordlander, P.; Halas, N. J. *Acc. Chem. Res.* **2007**, *40*, 53−62.
(17) Le, F.; Lwin, N.; Steele, J.; Käll, M.; Halas, N.; Nordlander, P. *Nano Lett.* **2005**, *5*, 2009−2013.
(18) Hao, F.; Nordlander, P. *Appl. Phys. Lett.* **2006**, *89*, 103101.
(19) Sun, Y. G.; Yin, Y. D.; Mayers, B. T.; Herricks, T.; Xia, Y. N. *Chem. Mater.* **2002**, *14*, 4736−4745.
(20) Laroche, T.; Girard, C. *Appl. Phys. Lett.* **2006**, *89*, 233119.

NL071001T